Augmented space recursion formulation of the study of disordered alloys with noncollinear magnetism and spin-orbit coupling: Application to MnPt and Mn_3Rh

Shreemoyee Ganguly,[1] Marcio Costa,[2,3] Angela B. Klautau,[4]
Anders Bergman,[3] Biplab Sanyal,[3] Abhijit Mookerjee,[1] and Olle Eriksson[3]
[1]*Department of Materials Science and Advanced Materials Research Unit, S. N. Bose National Centre for Basic Sciences, Block JD, Sector III, Salt Lake, Kolkata 700098, India*
[2]*Instituto de Fisica, Universidade Federal Fluminense, 24210-346 Niteri, Rio de Janeiro, Brazil*
[3]*Division of Materials Theory, Department of Physics and Astronomy, Uppsala University, Box 516, S-751 20 Uppsala, Sweden*
[4]*Universidade Federal Do Para, Avenida Augusto Correa 01, Campus Bsico do Guam, CEP 66075-110, Belem, Pará, Brazil*
(Received 18 November 2010; revised manuscript received 11 January 2011; published 10 March 2011)

We have developed a formalism by combining the tight binding linearized muffin-tin orbital and the recursion methods with the augmented space formalism (TB-LMTO-ASR) to study noncollinear magnetism in disordered alloys. We apply the TB-LMTO-ASR to study disordered MnPt and Mn_3Rh alloys. The electronic structures of these alloys in different magnetic structures have been calculated and compared to the previous theoretical results.

DOI: 10.1103/PhysRevB.83.094407 PACS number(s): 71.15.Mb, 36.40.Cg, 75.50.Pp

I. INTRODUCTION

Antiferromagnetic materials have attracted attention because of their potential candidature for giant magnetoresistance (GMR) devices. From a microscopic viewpoint, it is interesting to examine how lattice structure, composition, long-ranged disorder, and short-range ordering determine the magnetic structure of antiferromagnetic alloys. In many random alloys with close-packed lattice configurations, magnetic structures can become quite complex as compared to the simple collinear antiferromagnetic picture usually assumed. Atomic arrangement and randomness may introduce frustration effects in such alloys. Neutron diffraction experiments have often suggested complex magnetic alignments in mostly Mn-based disordered alloys like FeMn, MnPt, Mn_3Pt, and Mn_3Rh due to the presence of almost half-filled Mn $3d$ orbitals. Noncollinear magnetism has been studied within the density functional theory in formalisms, where the energies are functionals not of charge density but density matrices in spinor space. This has been done for ordered alloys,[1–3] amorphous materials,[4,5] and disordered alloys[6,7] based on both the Korringa-Kohn-Rostocker (KKR) and linear muffin-tin orbitals (LMTO) methods, coupled with the single-site coherent potential approximation (CPA) to deal with disorder.

In this work we propose to generalize the augmented space recursion[8] (ASR) based on the tight-binding version of the LMTO (TB-LMTO) so that it is capable of describing noncollinear magnetism. Local magnetic moments in alloys are strongly affected by the disorder in their local environments. Our aim will be to suggest a formalism which will allow us to go beyond the usual single-site mean-field approximations and provide an analyticity and symmetry-preserving generalization capable of addressing the situations where disorder fluctuations in the environment are important (like clustering or short-ranged ordering) accurately.

The rest of the paper is arranged as follows. In Sec. II we briefly discuss the Kohn-Sham equation generalized within the density-matrix functional theory to take care of noncollinear magnetism. Subsequently, we obtain a representation of the Kohn-Sham "Hamiltonian" in the TB-LMTO basis. In Sec. III we introduce substitutional disorder and the augmented space formalism to take care of configuration averaging. In Sec. IV we briefly describe the scalar recursion method. Finally, in Sec. V we shall apply our formalism to study the possibility of noncollinear magnetism in disordered MnPt and Mn_3Rh alloys.

II. BASIC FORMULATION

A. The Kohn-Sham equation with noncollinear magnetism

Since our aim is to study alloys via the ASR technique, we would like to develop a methodology which gives rise to a sparse Hamiltonian representation with matrix elements obtained self-consistently through a density functional formulation. The generalization of the collinear local spin-density approximation (LSDA) begins at the level of the Kohn-Sham equation. The Kohn-Sham orbitals in a spin-polarized electron liquid are spinors of the form

$$\underline{\underline{\psi}}(E,\vec{r}) = \begin{pmatrix} \psi_1(E,\vec{r}) \\ \psi_2(E,\vec{r}) \end{pmatrix}.$$

The magnetization density, like the charge density, is a local function. We describe our system on a more coarse-grained level. We start with the "rigid spin approximation" in which we associate with each Wigner-Seitz cell (or atomic sphere if we use the atomic sphere approximation) labeled by $\vec{R}$ a unique direction of magnetization. This direction will be the *local* quantization axis characterized by two angles θ_R, ϕ_R with respect to a set of suitably chosen global axes. With respect to these global axes the Kohn-Sham equation may be written as

$$\left\{\left(-\frac{1}{2}\nabla^2\right)\mathbf{I} + \mathbf{V}^{\mathrm{KS}}(\vec{r})\right\}\underline{\underline{\psi}}(E,\vec{r}) = E\underline{\underline{\psi}}(E,\vec{r}), \qquad (1)$$

where the effective Kohn-Sham potential is

$$\mathbf{V}^{\mathrm{KS}}(\vec{r}) = \sum_R \{V_{\mathrm{Hart}}(\vec{r}_R) + V_{\mathrm{ie}}(\vec{r}_R) + V_{\mathrm{SR}}(\vec{r}_R)\}\mathbf{I} + \mathbf{V}_{\mathrm{xc}}(\vec{r}_R) + v(r)\,\vec{L}\cdot\vec{\mathbf{S}}, \qquad (2)$$

where, $\vec{r}_R = \vec{r} - \vec{R}$, $V_{\rm Hart}(\vec{r}_R)$ is the Hartree potential, $V_{\rm ie}(\vec{r}_R)$ the ion-electron potential, and $V_{SR}(\vec{r}_R)$ is the scalar relativistic correction. $\mathbf{V}_{\rm xc}(\vec{r}_R) = V_{\rm xc}^{(1)}\mathbf{I} + \vec{B}\cdot\vec{\mathbf{S}}$ is the exchange-correlation potential, where

$$\vec{B}(\vec{r}) = \sum_R V_{\rm xc}^{(2)}(\vec{r}_R)\ \vec{e}_R,$$

in which $\vec{e}_R$ is the unit vector along the direction of the local quantization axis within the Rth Wigner-Seitz cell.

The Kohn-Sham Hamiltonian acts on the Hilbert space $\mathcal{H}\otimes\mathcal{S}$, where $\mathcal{S}$ is the spin space spanned by the bispinors

$$\begin{pmatrix}1\\0\end{pmatrix} \text{and} \begin{pmatrix}0\\1\end{pmatrix}.$$

$\vec{\mathbf{S}}$ are spin operators in the space $\mathcal{S}$.

The local and global spinor bases are related to each other through the SU(2) rotation matrix

$$\mathcal{U} = \begin{pmatrix} e^{i\phi_R/2}\cos(\theta_R/2) & e^{-i\phi_R/2}\sin(\theta_R/2) \\ -e^{i\phi_R/2}\sin(\theta_R/2) & e^{-i\phi_R/2}\cos(\theta_R/2)\end{pmatrix}.$$

In the local axes, the exchange-correlation potential $\mathbf{V}_{\rm xc}(\vec{r}_R)$ can be diagonalized in spinor space:

$$\mathcal{U}^\dagger\,\mathbf{V}_{\rm xc}(\vec{r}_R)\,\mathcal{U} = \begin{pmatrix} V_{\rm xc}^{\uparrow}(\vec{r}_R) & 0 \\ 0 & V_{\rm xc}^{\downarrow}(\vec{r}_R)\end{pmatrix}.$$

$V_{\rm xc}^{\sigma}(\vec{r}_R) = \delta E_{\rm xc}/\delta\rho^{\sigma}(\vec{r}_R)$ is the exchange-correlation potential referred to local quantization axes referred to by $\sigma = \uparrow, \downarrow$ in the Wigner-Seitz cell labeled by R. Furthermore,

$$\begin{aligned} V_{\rm xc}^{(1)}(\vec{r}_R) &= \tfrac{1}{2}\{V_{\rm xc}^{\uparrow}(\vec{r}_R) + V_{\rm xc}^{\downarrow}(\vec{r}_R)\}, \\ V_{\rm xc}^{(2)}(\vec{r}_R) &= \tfrac{1}{2}\{V_{\rm xc}^{\uparrow}(\vec{r}_R) - V_{\rm xc}^{\downarrow}(\vec{r}_R)\}. \end{aligned} \tag{3}$$

The spin-orbit potential, suitably spheridized within a muffin tin is related to the spheridized Kohn-Sham potential in the absence of relativistic corrections via

$$v(r) = \frac{1}{r}\frac{dV_{KS}(r)}{dr}.$$

The use of this potential in describing the spin-orbit part has been discussed by Koelling and Harmon.[9] Stiles *et al.*[10] have argued that a more systematic approach incorporates two-body terms of the type introduced by Breit.[11] This approach introduces not only the standard term given by us, but also a spin-other-orbit interaction, off diagonal in real space. This we have neglected for the time being in this work.

B. The TB-LMTO Hamiltonian

The Kohn-Sham equation can be represented in different bases. We choose the TB-LMTO in the maximally screened (or α) representation. Our choice is guided by the fact that the TB-LMTO-α representation of the Hamiltonian is sparse. This is essential both for modeling substitutional disordered alloys and for the recursion method (which we subsequently use) to be computationally tractable.

The TB-LMTO basis is now set up in the usual way[12] and applied to the above Kohn-Sham equation. The secular equation then leads to the TB-LMTO Hamiltonian

$$\mathbf{H} = H^{(0)}\mathbf{I} + \vec{B}\cdot\vec{\mathbf{S}} + \mathbf{H}_{\rm SO},$$

where the second-order spin-independent Hamiltonian is given by

$$H^{(0)} = E_v + h^\alpha - h^\alpha\, o^\alpha\, h^\alpha.$$

$H^{(0)}$ is an operator in the space $\mathcal{H}$ spanned by the LMTO basis $|RL\rangle$ and

$$\begin{aligned} h^\alpha_{RL,R'L'} = \{C^{(1)}_{RL} - E_{v\ell}\}\delta_{RR'}\delta_{LL'} + \Delta^{(1)1/2}_{RL} S_{RL,R'L'}\Delta^{(1)1/2}_{R'L'} \\ + \Delta^{(2)1/2}_{RL} S_{RL,R'L'}\Delta^{(2)1/2}_{R'L'}(\vec{e}_R\cdot\vec{e}_{R'}). \end{aligned} \tag{4}$$

The potential parameters referred to the local quantization axes are $\Pi_{RL} \equiv \{C^{\uparrow}_{RL}, C^{\downarrow}_{RL}, \Delta^{\uparrow 1/2}_{RL}, \Delta^{\downarrow 1/2}_{RL}, o^{\uparrow}_{RL}$ and $o^{\downarrow}_{RL}\}$. Referred to the global axes these parameters transform to $\Pi^{(1)}_{RL} = (\Pi^{\uparrow}_{RL} + \Pi^{\downarrow}_{RL})/2$ and $\Pi^{(2)}_{RL} = (\Pi^{\uparrow}_{RL} - \Pi^{\downarrow}_{RL})/2$. $S_{RL,R'L'}$ is the screened structure matrix, short ranged in $|R-R'|$. The vector $\vec{e}_R$ is a unit vector in the direction of the local moment in the atomic sphere labeled by R:

$$\begin{aligned} \vec{B}_{RL,R'L'} = \big(C^{(2)}_{RL} + \Delta^{(2)1/2}_{RL} S_{RL,R'L'}\Delta^{(1)1/2}_{R'L'}\big)\vec{e}_R \\ + \big(\Delta^{(1)1/2}_{RL} S_{RL,R'L'}\Delta^{(2)1/2}_{R'L'}\big)\vec{e}_{R'} \\ + \big(\Delta^{(2)1/2}_{RL} S_{RL,R'L'}\Delta^{(2)1/2}_{R'L'}\big)(\vec{e}_R\times\vec{e}_{R'}). \end{aligned} \tag{5}$$

When all spins in every Wigner-Seitz cell are collinear, $\vec{e}_R = \hat{z}$ for all R, then the first two terms in the Hamiltonian expression reduces to the usual LSDA expression, diagonal in the spinor space $\mathcal{S}$. Otherwise, the Hamiltonian has off-diagonal elements in $\mathcal{S}$:

$$\mathbf{H}_{\rm SO} = \Lambda^+\mathbf{S}^- + \Lambda^-\mathbf{S}^+ + \Lambda^z\mathbf{S}_z.$$

Further,

$$\begin{aligned} \Lambda^+_{LR,L'R'} &= v_{R,LL'}N^+_L\ \delta_{RR'}\ \delta_{\ell,\ell'}\ \delta_{m',m+1}, \\ \Lambda^-_{LR,L'R'} &= v_{R,LL'}N^-_L\ \delta_{RR'}\ \delta_{\ell,\ell'}\ \delta_{m',m-1}, \\ \Lambda^z_{LR,L'R'} &= v_{R,LL'}m\ \delta_{RR'}\ \delta_{\ell,\ell'}\ \delta_{m,m'}, \end{aligned} \tag{6}$$

with

$$\begin{aligned} N^+_L &= \sqrt{(\ell-m)(\ell+m+1)}, \\ N^-_L &= \sqrt{(\ell+m)(\ell-m+1)}. \end{aligned}$$

The representation of the Green's function in spinor space is a two-by-two matrix: $G^{\alpha\alpha'}_{RL,R'L'}$.

The magnetic density of states is given by

$$\vec{m}_{RL}(E) = -\frac{1}{\pi}\,\mathrm{Im}\,\mathrm{Tr}_\alpha\{\vec{\mathbf{S}}\mathbf{G}_{RL,RL}(E+i0)\}. \tag{7}$$

Within the rigid moment approximation, the magnetic moment in the Wigner-Seitz cell labeled by R is

$$\vec{m}_R = \sum_L \int_{-\infty}^{E_F} dE\ \vec{m}_{RL}(E). \tag{8}$$

The unit vectors defined earlier are $\vec{e}_R = \vec{m}_R/m_R$.

The effective exchange energy, which is the amplitude of the exchange field acting at a site labeled by R by the surrounding moments, is $J_0 = \sum_{R''} J(R'')$, where $R'' = R - R'$ and $J(R-R')$ is the pair energy given by the Lichtenstein formula,[13]

$$\begin{aligned} J(R-R') = -\frac{1}{4\pi}\mathrm{Im}\int_{-\infty}^{E_F}\sum_{LL'}\Big\{\delta_{RL}(E)\,G^{\uparrow\uparrow}_{RL,R'L'}(E)\delta_{R'L'} \\ \times(E)\,G^{\downarrow\downarrow}_{R'L',RL}(E)\Big\}, \end{aligned} \tag{9}$$

where $\delta_{RL}(E) = \Pi^{\uparrow}_{RL}(E) - \Pi^{\downarrow}_{RL}(E)$ and $\Pi^{\sigma}_{RL}(E) = (E - C^{\sigma}_{RL})/\Delta^{\sigma}_{RL}$.

C. The augmented space formalism and the augmented space Hamiltonian

The augmented space formalism was introduced by one of us[8] as a methodology to obtain configuration averages of functions of a set of random variables directly. Since there have been numerous and detailed descriptions of the methodology already,[14] we shall direct the curious reader to the review referred to above. Here we only describe the functional steps necessary to implement the technique.

Suppose a representation of the Hamiltonian of the disordered binary alloy in a denumerable basis $\{|RL\rangle\}$ involves random potential parameters Π_{RL}. For a substitutional, binary random alloy, this can be written in terms of a random "occupation" variable n_R as

$$\Pi_{RL} = \Pi_{AL}\, n_R + \Pi_{BL}\,(1 - n_R) = \Pi_{BL} + \Delta\Pi_L\, n_R,$$

where

$$n_R = \begin{cases} 1 \text{ if } R \text{ is occupied by atom } A \text{ with probability } x_A, \\ 0 \text{ if } R \text{ is occupied by atom } B \text{ with probability } x_B, \end{cases}$$

and $\Delta\Pi_L = \Pi_{AL} - \Pi_{BL}$ and the probability density of n_R is $p(n_R) = x_A\delta(n_R - 1) + x_B\delta(n_R)$.

In the augmented space formalism, we associate with the random variable n_R an operator M_R, such that its eigenvalues are the values taken by n_R and its spectral density is the probability density of n_R. The "configuration space" of n_R, Φ_R, is the space spanned by the eigenvectors of M_R. For a binary variable taking two values A and B, the configuration space of n_R, Φ_R, is of rank 2 and is spanned by the configurations $\{|A_R\rangle$ and $|B_R\rangle\}$.

It is more convenient to change to a new basis $|0_R\rangle = \sqrt{x_A}|A_R\rangle + \sqrt{x_B}|B_R\rangle$ and $|1_R\rangle = \sqrt{x_B}|A_R\rangle - \sqrt{x_A}|B_R\rangle$.

In this basis, the representation of M_R is

$$M_R = x_A\, I + (x_B - x_A)\, P^{(1)}_R + \sqrt{x_A x_B}\, T^{(01)}_R \in \Phi_R,$$

with $P^{(1)}_R = |1_R\rangle\langle 1_R|$ and $T^{(01)}_R = |1_R\rangle\langle 0_R| + |0_R\rangle\langle 1_R|$.

For each random variable n_R we introduce an operator M_R in this way. The *configuration space* of the set of random variables $\{n_R\}$ is $\Phi = \prod^{\otimes}\Phi_R$.

The augmented space theorem[8] states that the configuration average of any function $f(\{n_R\})$ may be written as

$$\ll f(\{n_R\}) \gg = \langle\{\emptyset\}|\tilde{f}(\{\widetilde{M}_R\})|\{\emptyset\}\rangle \tag{10}$$

where $\tilde{f}(\{\widetilde{M}_R\})$ is the same operator function of the operators $\{\widetilde{M}_R\}$ as $f(\{n_R\})$ was of $\{n_R\}$. Operationally, we construct the operator $\tilde{f}(\{\widetilde{M}_R\})$ by replacing each n_R in $f(\{n_R\})$ by the corresponding $\widetilde{M}_R$. Further, $|\{\emptyset\}\rangle = \prod^{\otimes}_R |0_R\rangle$, and $\widetilde{M}_R = I \otimes \cdots I \otimes M_R \otimes \cdots \in \Phi$. All tilded operators acts on the configuration space Φ.

If we substitute this back into the expression for the potential parameters Π_{RL} we get an associated operator in configuration space,

$$\widetilde{\Pi}_{RL} = \ll \Pi_L \gg \tilde{I} + \mathcal{B}(\Pi_L)\, \widetilde{P}^{(1)}_R + \mathcal{F}(\Pi_L)\, \widetilde{T}^{(01)}_R, \tag{11}$$

where $\mathcal{B}(\Pi_L) = (x_B - x_A)\,\Delta\Pi_L$ and $\mathcal{F}(\Pi_L) = \sqrt{x_B x_A}\,\Delta\Pi_L$, $\Delta\Pi_L = \Pi_{AL} - \Pi_{BL}$.

We can now start from Eqs. (4) and (5) and rewrite the Hamiltonian as an operator in the Hilbert space $\mathcal{H}$, spanned by the TB-LMTO basis $\{|RL\rangle\}$. We now allow each potential parameter to be random. Referring to Eq. (11) we can construct the Hamiltonian in *augmented space* $\Psi = \mathcal{H} \otimes \Phi$:

$$\widehat{h}^{\alpha} = \sum_{RL} \widetilde{A}_{RL} \otimes P_{RL} + \sum_{RL,R'L'} \left\{ \widetilde{B}^{(1)}_{RL,R'L'} \otimes T_{RL,R'L'} + \left(\widetilde{B}^{(2)}_{RL,R'L'} \otimes T_{RL,R'L'}\right) \sum_{\mu} e^{\mu}_R e^{\mu}_{R'} \right\},$$

$$\widehat{B}^{\mu} = \sum_{RL} \left(\widetilde{D}_{RL} \otimes P_{RL} + \sum_{R'} \widetilde{B}^{(3)}_{RL,R'L'} \otimes T_{RL,R'L'} \right) e^{\mu}_R + \sum_{RL,R'L'} \left\{ \left(\widetilde{B}^{(4)}_{RL,R'L'} \otimes T_{RL,R'L'}\right) e^{\mu}_{R'} + \left(\widetilde{B}^{(2)}_{RL,R'L'} \otimes T_{RL,R'L'}\right) \sum_{\nu\xi} \varepsilon^{\mu\nu\xi}\, e^{\nu}_R e^{\xi}_{R'} \right\},$$

where

$$\begin{aligned}
\widetilde{A}_{RL} &= \widetilde{C}^{(1)}_{RL} - \widetilde{E}_{\nu L}; \quad \widetilde{D}_{RL} = \widetilde{C}^{(2)}_{RL}; \\
\widetilde{B}^{(1)}_{RLR'L'} &= \widetilde{\Delta}^{(1)\,1/2}_{RL} \otimes \tilde{S}_{RLR'L'} \otimes \widetilde{\Delta}^{(1)\,1/2}_{R'L'}; \\
\widetilde{B}^{(2)}_{RLR'L'} &= \widetilde{\Delta}^{(2)\,1/2}_{RL} \otimes \tilde{S}_{RLR'L'} \otimes \widetilde{\Delta}^{(2)\,1/2}_{R'L'}; \\
\widetilde{B}^{(3)}_{RLR'L'} &= \widetilde{\Delta}^{(2)\,1/2}_{RL} \otimes \tilde{S}_{RLR'L'} \otimes \widetilde{\Delta}^{(1)\,1/2}_{R'L'}; \\
\widetilde{B}^{(4)}_{RLR'L'} &= \widetilde{\Delta}^{(1)\,1/2}_{RL} \otimes \tilde{S}_{RLR'L'} \otimes \widetilde{\Delta}^{(2)\,1/2}_{R'L'}.
\end{aligned}$$

Here P_{RL} and $T_{RL,R'L'}$ are projection and transfer operators, respectively, in the Hilbert space $\mathcal{H}$ spanned by the TB-LMTO basis $\{|RL\rangle\}$. All hatted operators act on the full augmented space Ψ. Thus,

$$\widehat{H}^{(0)} = \widehat{E}_{\nu} + \widehat{h}^{\alpha} - \widehat{h}^{\alpha} \otimes \widehat{o}^{\alpha} \otimes \widehat{h}^{\alpha},$$

where

$$\widehat{E}_{\nu} = \widetilde{E}_{\nu\, L} \otimes I, \qquad \widehat{o}^{\alpha} = \sum_{RL} \widetilde{o}_{RL} \otimes P_{RL}.$$

Similarly, for the spin-orbit part,

$$\widehat{\Lambda}^{+} = \sum_{RL} \widetilde{v}^{+}_L \otimes P_{RL}, \qquad \widehat{\Lambda}^{-} = \sum_{RL} \widetilde{v}^{-}_L \otimes P_{RL},$$

$$\widehat{\Lambda}^{z} = \sum_{RL} \widetilde{v}^{z}_L \otimes P_{RL}.$$

So that the full augmented space Hamiltonian becomes

$$\widehat{\mathbf{H}} = \widehat{H}^{(0)}\mathbf{I} + \sum_{\mu} \widehat{B}^{\mu}\, \mathbf{S}^{\mu} + \widehat{\Lambda}^{+}\mathbf{S}^{-} + \widehat{\Lambda}^{-}\mathbf{S}^{+} + \widehat{\Lambda}^{z}\mathbf{S}^{z}. \tag{12}$$

The augmented space theorem then gives the averaged Green's function as

$$\ll \mathbf{G}_{RL,R'L'}(E) \gg = \langle RL\{\emptyset\}| \, \widehat{\mathbf{G}}(E) \, |R'L'\{\emptyset\}\rangle, \tag{13}$$

where

$$\widehat{\mathbf{G}}(E) = \left(E\hat{\mathbf{I}} - \widehat{\mathbf{H}}\right)^{-1} \in \Psi,$$

and $|RL\{\emptyset\}\rangle = |RL\rangle \otimes |\{\emptyset\}\rangle$ is a particular state in augmented space Ψ.

The averaged projected and magnetic density of states are

$$\ll n_{RL}(E) \gg = -\frac{1}{\pi} \mathrm{Im}\ \mathrm{Tr}_\alpha \{\widehat{\mathbf{G}}_{RL\{\emptyset\},RL\{\emptyset\}}(E + i0)\},$$
$$\ll \vec{m}_{RL}(E) \gg = -\frac{1}{\pi} \mathrm{Im}\ \mathrm{Tr}_\alpha \{\vec{\mathbf{S}}\, \widehat{\mathbf{G}}_{RL\{\emptyset\},RL\{\emptyset\}}(E + i0)\}. \tag{14}$$

Among methods to deal with disorder, the most used is the single-site, mean-field, CPA. This approximation has been eminently successful in dealing with a variety of disordered systems. Of all the single-site approximations, the CPA alone maintains the essential Herglotz[15] analytical properties and lattice translational symmetry of the averaged Green's function. In earlier works we have shown[16,17] that the CPA can be obtained as a specific approximation within the augmented space formalism. Ordinarily, the ASR will subsume the CPA. However, wherever effects of statistical clustering,[18] short-ranged ordering,[19,20] partial or sublattice disorder,[21] and off-diagonal disorder arising out of local lattice distortions due to large size mismatch of constituent atoms in the alloy[22] become important, the ASR provides an analyticity and symmetry preserving generalization to the CPA capable of addressing these situations accurately. These local environmental effects strongly affect the local magnetic moments. One of the aims of this work is to put forward a formalism that will allow us to go beyond the single-site CPA and take into account environmental effects.

Of the generalizations of the CPA, the augmented space-based methods—the traveling cluster approximation (TCA),[23,24] the itinerant CPA[25] (ICPA), and the ASR[26]—are among the most successful. They too not only retain the necessary analytic (Herglotz) properties and lattice translational symmetry of the averaged Green's function, as the CPA does, but also properly incorporate local environment effects. We have chosen the ASR. In particular, a recursion carried out till n steps before termination yields $2n$ moments of the density of states accurately and samples an environment n steps away from the starting state.

D. The recursion method in augmented space

One of the useful $O(N)$ methods for the calculation of the Green's function in systems where lattice translation symmetry is broken is the recursion method proposed by Haydock *et al.*[27] The augmented space theorem tells us that the Green's functions calculated with the full augmented space Hamiltonian (described above) and projected onto the configuration subspace spanned by $|\{\emptyset\}\rangle = \prod_R^{\otimes} |0_R\rangle$ is the configuration averaged Green's function. The result is exact, and therefore, if we obtain the averaged Green's function by the recursion method, the only approximations will be those related to the *termination* of the continued fraction. Haydock and co-workers[28] and Beer and Pettifor[29] have described various analyticity preserving terminators. Unlike mean-field theories like the CPA and its cluster generalizations, these approximations are controlled and errors can also be easily estimated.[28]

In order to calculate a generalized noncollinear magnetization density, we need also to calculate the nondiagonal elements of the Green's function in spinor space.[30] At this point we may proceed in several different ways. Either we carry out three recursions with local quantization axis rotated in the x, y, or z directions by SU(2) rotation matrices or the nondiagonal elements of the Green's function can be calculated either by performing several recursions with carefully chosen starting states.[31] Alternately, we can perform vector recursion.[32,33] In this work we use the scalar recursion with rotated quantization axes. However, vector recursion is elegant and requires only a single application for both the diagonal and the off-diagonal Green's function spinor matrix elements. We postpone application of vector recursion for a later communication. The question of rotational invariance of the Green's function obtained from scalar recursion has been addressed by one of us in earlier works on the applications of recursion in studying noncollinear magnetism in ordered compounds.[30,34–36] Introduction of homogeneous disorder will not alter that line of argument. Maintaining rotational invariance of the Green's function comes naturally within the vector recursion method.

For the sake of completeness, we briefly describe the scalar recursion technique in the full augmented space.

If we do a rigid moment approximation within an atomic sphere, then we can define a local spin-axis in which $\mathbf{S}_z$ is diagonal. We can apply unitary SU(2) rotation operators $\mathcal{U}_x$, $\mathcal{U}_y$, and $\mathcal{U}_z = I$ which diagonalize $\mathbf{S}_x$, $\mathbf{S}_y$, and $\mathbf{S}_z$, respectively. Thus,

$$\begin{aligned}
&\ll m^\mu_{RL}(E) \gg \\
&\quad = -\frac{1}{\pi} \mathrm{Im}\ \mathrm{Tr}\{\mathbf{S}^\mu\, \mathcal{U}^\dagger_\mu \mathcal{U}_\mu\, \mathbf{G}_{RL\{\emptyset\},RL\{\emptyset\}}(E)\, \mathcal{U}^\dagger_\mu \mathcal{U}_\mu\} \\
&\quad = -\frac{1}{\pi} \mathrm{Im}\ \mathrm{Tr}\{(\mathcal{U}_\mu \mathbf{S}^\mu \mathcal{U}^\dagger_\mu)\, (\mathcal{U}_\mu \mathbf{G}_{RL\{\emptyset\},RL\{\emptyset\}}(E) \mathcal{U}^\dagger_\mu)\} \\
&\quad = -\frac{1}{\pi} \mathrm{Im}\ \mathrm{Tr}\{\mathbf{S}'_\mu\, \mathbf{G}'_{RL\{\emptyset\},RL\{\emptyset\}}(E)\}
\end{aligned}$$

and

$$\ll m^\mu_R \gg = \sum_L \int_{-\infty}^{E_F} dE \ll m^\mu_{RL}(E) \gg . \tag{15}$$

Since $\mathbf{S}'_\mu$ are diagonal in spinor space we need to calculate only the diagonal elements of $\mathbf{G}'_{RL\{\emptyset\},RL\{\emptyset\}}$. This requires two recursions per direction, so six recursions in all. Moreover,

$$\widehat{\mathbf{G}}'(E) = (E\hat{\mathbf{I}} - \widehat{\mathbf{H}}')^{-1} \in \Psi,$$

where

$$\widehat{\mathbf{H}}' = \widehat{H}^{(0)}\mathbf{I} + \sum_\mu \widehat{B}^\mu\, \mathbf{S}'^\mu + \widehat{\Lambda}^+ \mathbf{S}'^- + \widehat{\Lambda}^- \mathbf{S}'^+ + \widehat{\Lambda}^z \mathbf{S}'^z.$$

The recursion in full augmented space then follows: First, we have to have a representation of "states" in augmented

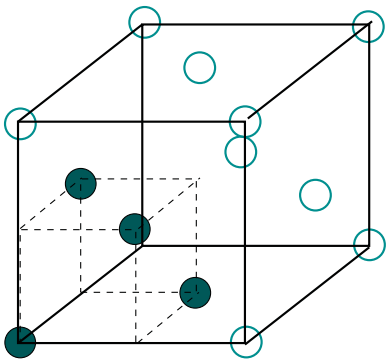

FIG. 1. (Color online) Choice of the magnetic primitive cell on a fcc lattice.

space. In the absence of disorder the representation is simple: A state is labeled by L and R. So we can represent this by a $(\ell_{\max}+1)^2 \times N$ matrix, where $\ell_{\max}$ is the maximum angular momentum labels in the TB-LMTO minimal basis (usually 9 for s, p, and d basis) and N is the maximum number of muffin tins considered in the recursion procedure. For spin degrees of freedom each scalar in this $(\ell_{\max}+1)^2 \times N$ matrix is replaced by a 1×2 spinor. So one such state may be represented by the symbol: $|\Phi^{\alpha}_{RL}\rangle$ with $R = 1,2,\ldots N$, $L = 1,2,\ldots(\ell_{\max}+1)^2$, and $\alpha = 1,2$.

The states in configuration space can be uniquely labeled by the *cardinality sequence*, that is, the sequence of sites $\{\mathcal{C}>$ where we have a state $|1_R\rangle$. For example, the configuration state

$$|0_{R_1},\ldots,1_{R_k},0_{R_{k+1}},\ldots,1_{R_\ell},\ldots\rangle \equiv |\{R_k,R_\ell,\ldots\}\rangle.$$

A state in the full augmented space is given by $\Phi = |\Phi^{\alpha}_{RL} \otimes \{\mathcal{C}\}\rangle$. The inner product is defined by

$$(\Psi \odot \Phi) = \sum_{RL\alpha} \Psi^{\alpha}_{RL}\Phi^{\alpha}_{RL}\,\delta(\mathcal{C},\mathcal{C}').$$

The recursion begins with a state

$$|0\rangle = \left|\Phi^{\alpha}_{RL} \otimes \{\emptyset\}\right\rangle. \tag{16}$$

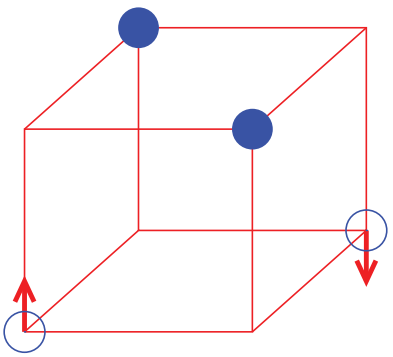

FIG. 2. (Color online) Collinear antiferromagnetism in ordered $L1_0$ MnPt. Mn atoms are shown as (blue) open circles while the Pt ions as (blue) solid circles.

The other states are generated from

$$\beta_{n+1}|n+1\rangle = \widetilde{\mathbf{H}}|n\rangle - \alpha_n|n\rangle - \beta_n|n-1\rangle. \tag{17}$$

Imposing orthogonality, one obtains

$$\alpha_n = \frac{\langle n|\widetilde{\mathbf{H}}|n\rangle}{\langle n|n\rangle} \quad \beta_n = \frac{\langle n-1|\widetilde{\mathbf{H}}|n\rangle}{\langle n-1|n-1\rangle}. \tag{18}$$

This new basis tridiagonalizes the Hamiltonian. It follows that

$$\begin{aligned} G^{(N)}(E) &= [E-\alpha_{N+1}-T(E)]^{-1}, \\ G^{(n)}(E) &= [E-\alpha_{n+1}-\beta^2_{n+1}G^{(n+1)}(E)]^{-1} \\ &\qquad \text{for} \quad n \leqslant N-1, \\ G^{(0)}(E) &= \ll G_{RL\alpha,RL\alpha}(E) \gg , \end{aligned} \tag{19}$$

where $T(E)$ is one of the terminators suggested by Haydock[28] or Beer and Pettifor.[29] Two recursions with the two possible starting states in Eq. (16) for the two values of α give the two diagonal matrix elements in spinor space.

III. APPLICATION TO MnPt ALLOYS

The ordered intermetallic compound 50-50 MnPt has a $L1_0$ structure. A small tetragonal distortion with $c/a \simeq 0.92$ lowers the total energy and stabilizes the compound. It exhibits collinear antiferromagnetism of the Mn atoms only. The Pt atoms carry negligible magnetic moment. The Néel temperature is rather high ≈1000 K.[37] Figure 1 shows the choice of the magnetic primitive cell for the alloys. For ordered MnPt alloy in the $L1_0$ structure the Mn and Pt atoms sit in alternate layers. This is shown in Fig. 2. It is experimentally known that the possible magnetic structure of Mn atoms is a AF-I type arrangement shown in Fig. 2.

Although ordered 50-50 MnPt has been studied earlier, not much work has been done on disordered 50-50 MnPt which has been prepared in thin film form. Interest in this alloy waned, primarily because the exchange bias mechanism is absent in them and therefore probability of their potential use in GMR devices is doubtful. Nevertheless, presence of possible antiferromagnetic Mn in the alloy and Pt which provides spin-orbit coupling makes this alloy system a fertile ground for a search for noncollinear magnetic phases.

In the disordered alloy, in contrast with the $L1_0$ ordered arrangement, the Mn and Pt atoms do not sit in parallel planes. The lattice structure is strictly face-centered cubic with both the corner and the face-center positions being occupied randomly with either Mn or Pt atoms with equal probability.

The magnetic arrangements on this face-centered lattice are shown in Fig. 3. The simplest is the $1Q$ arrangement where the intralayer alignment is collinear ferromagnetic while the interlayer alignment is antiferromagnetic. If we choose the positive c axis as the global axis of quantization (z axis) and represent the unit vector along the magnetic moment by $\vec{e}_R = (\theta_R,\phi_R)$, and if we label the position of the two sites on the bottom x-y plane as R_1,R_2 and those on the top x-y plane as R_3,R_4, then,

$$\begin{aligned} &\phi_{R_k} = 0^\circ, \quad \text{for} \quad k = 1,2,\ldots,4 \\ &\theta_{R_1} = \theta_{R_2} = 0^\circ; \quad \theta_{R_3} = \theta_{R_4} = 180^\circ. \end{aligned}$$

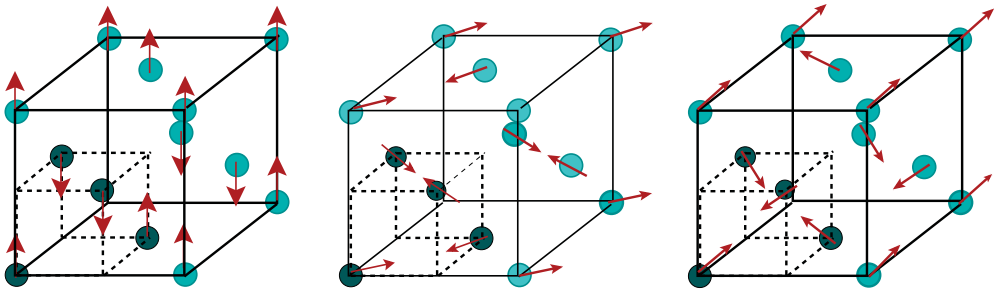

FIG. 3. (Color online) The $1Q$, $2Q$, and $3Q$ magnetic structures on the magnetic primitive lattice in a fcc structure.

The next arrangement is the $2Q$ noncollinear antiferromagnetic structure shown in the middle panel of Fig. 3. Here

$$\theta_{R_k} = 90^\circ, \quad \text{for} \quad k = 1,2,\ldots,4$$

$$\phi_{R_1} = 45^\circ, \quad \phi_{R_2} = 225^\circ, \quad \phi_{R_3} = 135^\circ, \quad \phi_{R_4} = 315^\circ.$$

The moments lie in planes in twos and point toward each other. Finally, the last arrangement is the $3Q$ structure shown in the rightmost panel of Fig. 3. This structure is quite similar to the $2Q$ with the difference that spins are raised in the lower plane and dipped in the upper plane so that now they all point toward the cube center.

$$\theta_{R_k} = 54.7^\circ \quad \text{for} \quad k = 1,2,\ldots,4,$$

$$\phi_{R_1} = 45^\circ, \quad \phi_{R_2} = 225^\circ, \quad \phi_{R_3} = 135^\circ, \quad \phi_{R_4} = 315^\circ.$$

We have carried out a fully self-consistent local density matrix functional approximation electronic structure and total energy calculation on all the three magnetic structures of the disordered MnPt alloy. We have chosen to carry out scalar recursions in the framework of the local quantization axes. We carried out 11 recursion steps on an augmented space cluster with seven nearest-neighbor shells around a central site. The terminator chosen was that of Beer and Pettifor.[29] The Madelung energy was estimated by the method of Ruban and Skriver.[38] The lattice constants of the ordered and disordered phases do not vary much and our presented calculations were done with $a = 3.77$ A. In Fig. 4 we present our partial (constituent projected) density of states (PDOS) results of our TB-LMTO-ASR calculations.

Before we discuss the disordered alloy, we remind the reader of the earlier work on the DOS of $L1_0$ AF-I MnPt (Ref. 7) and the related MnNi (Ref. 39) alloys. Both have a prominent pseudogap around the Fermi level. This has been assigned to the AF-I staggered field. This gap completely disappears in the ferromagnetic or paramagnetic arrangements. This pseudogap is absent in all the three disordered arrangements $1Q$, $2Q$, and $3Q$ of MnPt. The random arrangement of Mn and Pt atoms, which have electronic structures very different from each other, means that the regular $L1_0$ arrangement in the ordered phase is strongly disrupted as Pt and Mn randomly replace each other. This disrupts the AF-I staggered field and prevents a pseudogap forming near the Fermi level.

We need to comment on the accuracy of our ASR calculations. In particular, the accuracy of the dominant terminator approximation of the ASR. As Haydock has argued[28] that the DOS itself is unstable under small perturbations and convergence criteria need to be based on the convergence of the energy moments of the DOS: $M_n = \int_{E_{\min}}^{E_F} E^n \, n(E) \, dE$. Figure 5 shows the variation of the first four moments of the Mn PDOS for the $1Q$ magnetic states in MnPt, with the number of exact recursion steps before the asymptotic part of

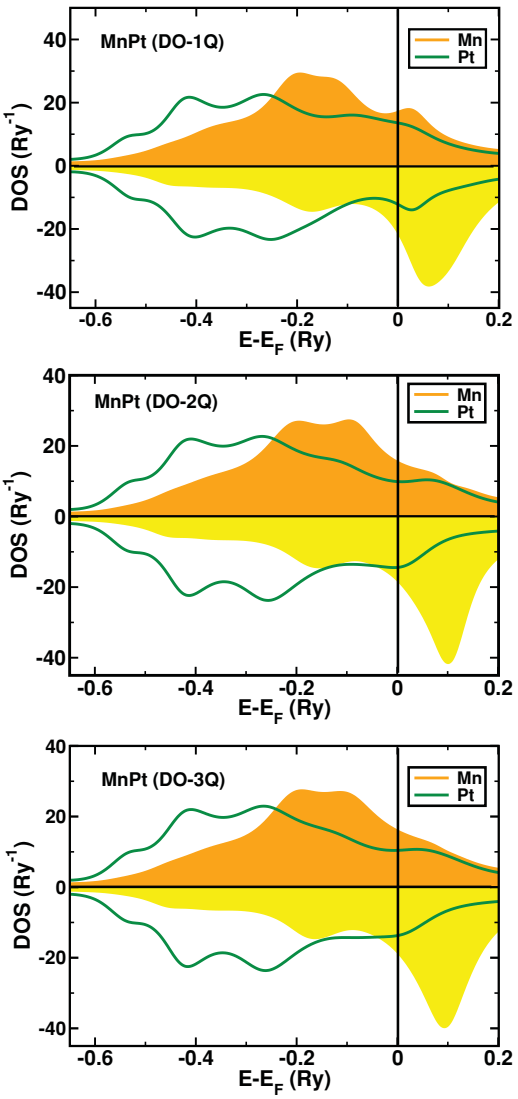

FIG. 4. (Color online) Partial density of states for Mn and Pt for the disordered (DO) $1Q$, $2Q$, and $3Q$ spin arrangements in MnPt alloys.

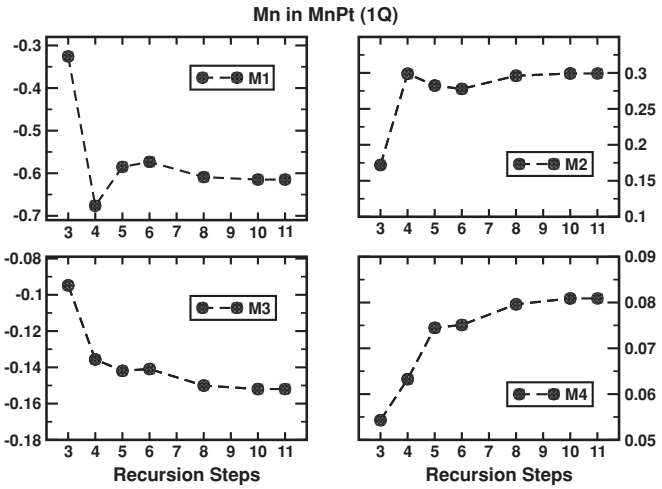

FIG. 5. Variation of the first four moments of the partial DOS of Mn in MnPt in the $1Q$ magnetic structure. The variation is with the number of recursion steps after which the asymptotic part of the continued fraction expression for the Green's function is replaced by a Beer-Pettifor terminator. The units for the moments M_n are $(\text{Ry})^n$.

the continued fraction expression for the Green's function is replaced (terminated) by a Beer-Pettifor "terminator." Results for the $2Q$ and $3Q$ magnetic states are qualitatively identical. We see that after 10–11 recursion steps the moments fluctuate by less than 5%. We have, therefore, terminated recursion after 11 steps with a sixth-nearest neighbor map in augmented space. Therefore, inaccuracy creeps up only in the 22nd moment, as opposed the 8th moment in the CPA. The Beer-Pettifor terminator ensures that the asymptotic moments are also accurate.

Table I shows the magnetic moments from our results and compares them with the CPA results of Sakuma.[7] The ASR agrees with the CPA that the $3Q$ arrangement has the lowest energy per atom. The CPA gave the $2Q$ arrangement to have almost the same energy as the $3Q$ arrangement and $1Q$ to be about 1.47 mRy/atom higher. The ASR, on the other hand, ordered the structures as $1Q$, 1.41 mRy/atom higher and then $2Q$ at 1.68 mRy/atom higher still. These energy differences of a few mRy/atom are really at the very limit of error windows of either the CPA or the ASR. The error occurs in the TB-LMTO and then in the single-site CPA or the better ASR approximation. These errors are additive and although

TABLE I. Magnetic moments obtained from TB-LMTO-CPA and TB-LMTO-ASR.

Spin structure	M^{a} (μ_B)	M^{b} (μ_B)
$1Q$	2.75	2.08
$2Q$	2.76	2.19
$3Q$	2.76	2.16

[a]TB-LMTO-CPA work by Sakuma (Ref. 7).
[b]Present work.

our earlier arguments convince us that the ASR is indeed more accurate than the CPA, we can only make definitive statements after transparent experimental evidence becomes available. The ASR estimates of the Mn moments are about 0.57–0.67 μ_B lower than the CPA.

IV. APPLICATION TO Mn_3Rh ALLOYS

The magnetic structure of ordered $L1_2$ Mn_3Rh is a complex triangular ($T1$) type shown in the left panel of Fig. 6. The structure was shown to be a stable structure of ordered Mn_3Rh by Kübler *et al.*[1] The central panel shows another coenergetic structure $T2$ while the right panel shows a collinear antiferromagnetic like structure. Like the earlier work of Kübler *et al.*, it was found that the $T1$ and $T2$ structures have the same DOS, total energies, and magnetic moments. As stated in that earlier work, this is expected since our theory does not couple magnetic moments to the underlying crystal lattice. What we focus on is the relative orientation of the moments. In this sense the $T1$ and $T2$ structures are identical. A similar argument was put forward by Bertaut and Fruchart[41] based on Heisenberg models for the $T1$ and the $T2$ structures. These are identical in the absence of anisotropy. We have therefore reported only the results for the $T1$ structure in what follows. The top panel of Fig. 7 shows the variation of the total energy with respect to the lattice constant. The figure shows that the $T1$ structure with $a = 3.62$ A is the stable ordered structure for Mn_3Rh. This is in consonance with the earlier work of Kübler *et al.*

The bottom panel of Fig. 7 shows the PDOS for Mn and Rh in the $T1/T2$ and collinear AFM structures. Both (particularly $T1$) indicate a pseudo-gap just above the Fermi level, as in MnPt. Otherwise the two PDOS are not very different from each other. Figure 8 shows the variation of magnetic

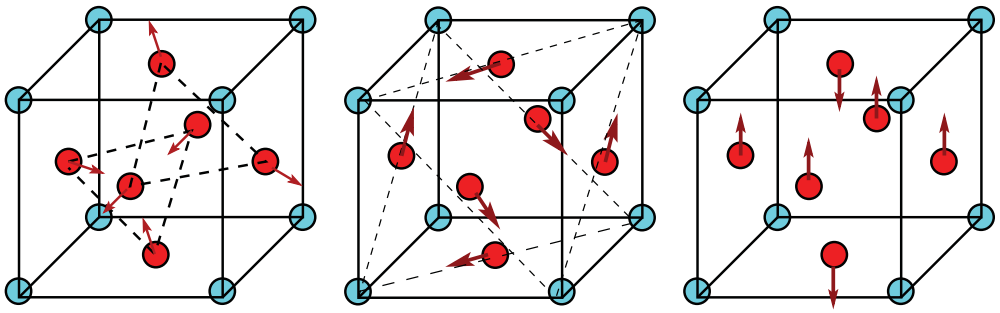

FIG. 6. (Color online) (Left) The $T1$ structure of $L1_2$ Mn_3Rh. (Center) The $T2$ structure of $L1_2$ Mn_3Rh. (Right) The collinear AFM structure of $L1_2$ Mn_3Rh. Red (dark gray) atoms are Mn and blue (light gray) atoms are Rh.

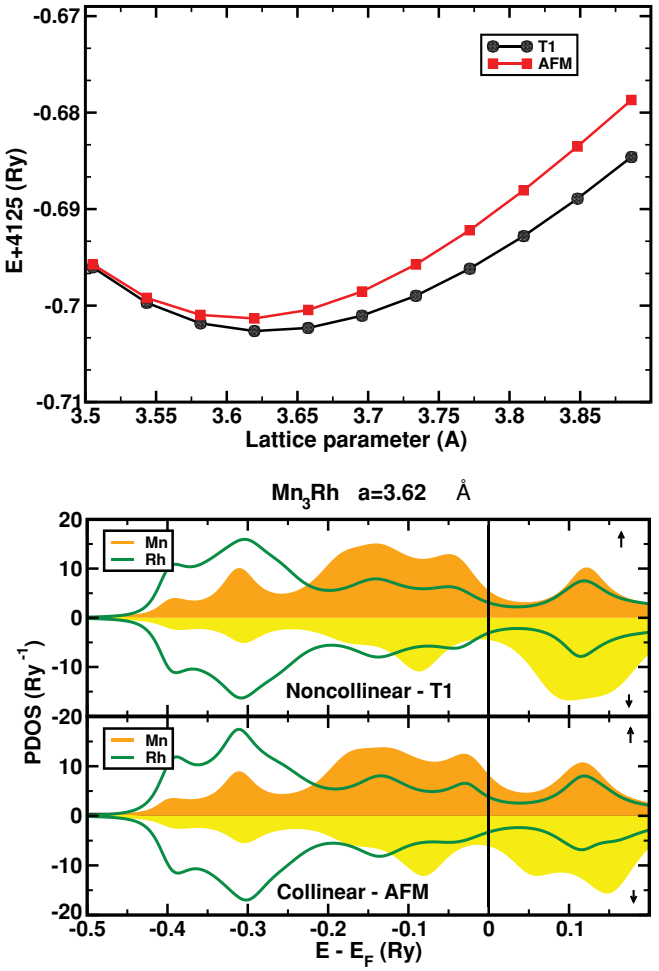

FIG. 7. (Color online) (Top) Total energy vs lattice constant for $T1$ and AFM structures for Mn_3Rh. (Bottom) PDOS for Mn and Rh for $T1/T2$ and collinear AFM Mn_3Rh.

moment with lattice constant for the $T1/T2$ and collinear AFM structures. The decrease of magnetic moment with lattice constant agrees with the Stoner criterion (since the closer the atoms, more is the overlap of electronic wave functions leading to a wider band and a lower DOS at the Fermi level). This indicates that these alloys exhibit itinerant magnetism. The estimate of the magnetic moment of $T1$ at equilibrium lattice

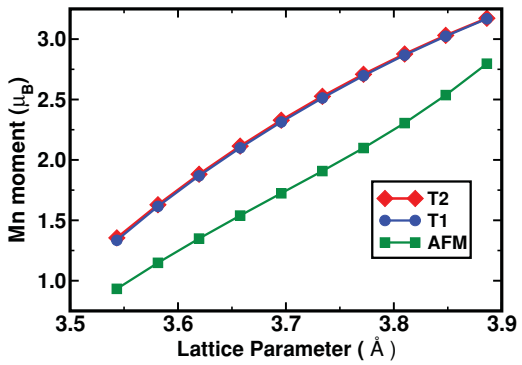

FIG. 8. (Color online) Magnetic moment variation with lattice constant for $T1/T2$ and collinear AFM Mn_3Rh.

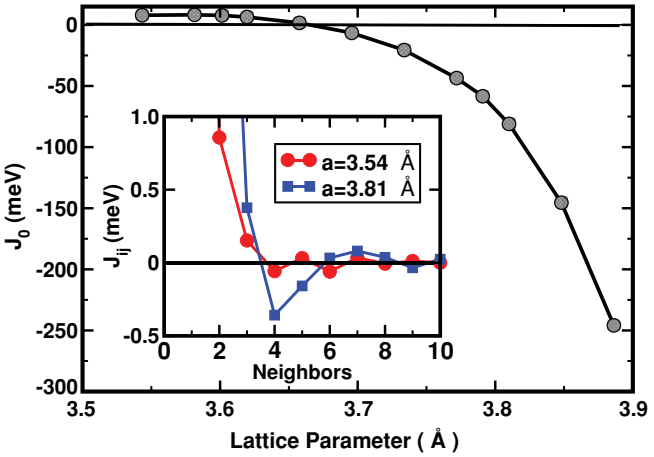

FIG. 9. (Color online) Exchange energy as a function of the lattice constant in $T1$ Mn_3Rh.

constant is not far from Sakuma *et al.*,[39] but smaller than that of Kübler *et al.*[2]

Figure 9 shows a rather interesting fact: The exchange energy changes sign on lattice expansion, going from antiferromagnetic to a ferromagnetic transition. The $T1$ arrangement at equilibrium lattice constant (3.62 A) sits almost at the edge of this transition.

Figure 10 shows the PDOS for Mn and Rh in Mn_3Rh in the $1Q$, $2Q$, and $3Q$ arrangements. The PDOS were calculated from the TB-LMTO-ASR using six nearest-neighbor shells in augmented space. The recursions were carried out exactly till 11 steps after which the Beer-Pettifor terminator was used to terminate the continued fraction. As in the case of MnPt, we show in Fig. 11 the convergence of the first four PDOS moments for Mn in $1Q$ Mn_3Rh. Again, those for $2Q$ and $3Q$ magnetic structures are qualitatively similar. The convergence is less monotonic as compared with MnPt. This is a reflection of the fact that the PDOS in Mn_3Rh has more structure as compared with MnPt. However, in this alloy system too, the convergence is good after 11 recursion steps and the fluctuation in moments is of the order of 5%. A glance at Fig. 10 indicates that in all the three disordered alloys, there is no vestige of a pseudogap near the Fermi level. Again, random substitution of Mn with Rh disrupts the $L12$ arrangement in the ordered structures and hence disrupting the effect of the staggered field. We note also that there is more structure to the Rh PDOS in Mn_3Rh as compared to Pt in MnPt and the overlap with the Mn PDOS is also greater.

Table II shows the results for magnetic moments from our work and compares them with the CPA. The magnetic moments from the ASR agree well with the CPA results. Rh, unlike Pt, now carries a small induced moment. However, while the CPA predicts stability in the order $3Q$, $2Q$, and $1Q$, the ASR predicts stability in the order $1Q$, $2Q$, and $3Q$. As we discussed earlier, these small energy differences between different magnetic structures are in the limits of our accuracy. Again, although we are confident that the ASR with recursion carried up to 11 steps before termination is more accurate than the single-site CPA, it would be useful to have definitive and transparent experimental results before we can make reliable statements.

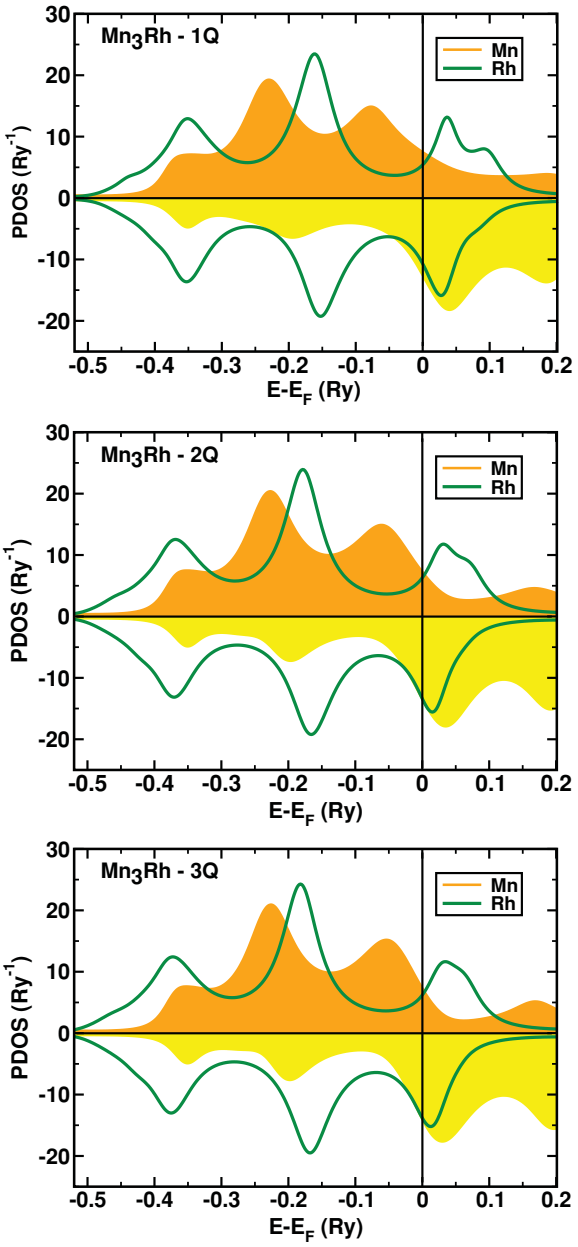

FIG. 10. (Color online) PDOS for the disordered Mn_3Rh alloy (top) $1Q$ structure, (middle) $2Q$ structure, and (bottom) $3Q$ structure.

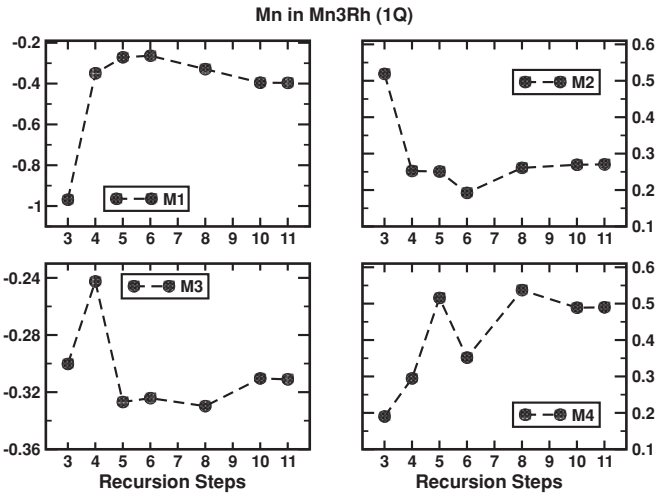

FIG. 11. Variation of the first four moments of the partial DOS of Mn in Mn_3Rh in the $1Q$ magnetic structure. The variation is with the number of recursion steps after which the asymptotic part of the continued fraction expression for the Green's function is replaced by a Beer-Pettifor terminator. The units for the moments M_n are $(\mathrm{Ry})^n$.

V. CONCLUSION AND REMARKS

We have set up a computational framework for the study of noncollinear magnetic phases in disordered alloys based on the marriage of three distinct techniques: the TB-LMTO, the recursion method, and the augmented space formalism. The ASR allows us to go beyond the single-site CPA and include effects of disorder in the local environment accurately. This is important, since the immediate environment of a magnetic atom in a solid has a significant impact on its local magnetic moment.

We have used our formalism to study disordered MnPt and Mn_3Rh alloys. Our ASR results are different from the earlier CPA, specially in the energy ordering of different noncollinear states. The very small energy differences between different noncollinear phases means that our error window should be very narrow. The augmented space formalism is formally exact; therefore, the error arises in the recursion method and the TB-LMTO. Errors in the former are controlled and can be estimated. The main source of error is in the TB-LMTO. A way out is either to replace TB-LMTO with the more accurate TB-KKR. This would lead to energy-dependent potential parameters and hence energy-dependent recursion. This was developed by us earlier.[42] Alternatively, we can use the full-potential LMTO. However, in that case, the Hamiltonian is not sparse and we have to have a relook at the errors in the recursion method. This work is now in progress.

In this paper we have started with a given noncollinear magnetic structure and used our technique to obtain its total energy and local magnetic moments. However, the formalism suggested by us can deal with situations where we may start with arbitrary local vector magnetic moments and carry out a full density functional self-consistent calculations based on charge densities and vector magnetic moment densities [via Eq. (15)]. In other words, during our self-consistency cycle we can relax the local magnetic moment directions. This is a generalization of the usual local spin-density functional theory (LSDA) for collinear magnetism. We have already carried out such calculations for ordered compounds

TABLE II. Magnetic moments obtained from TB-LMTO-CPA and TB-LMTO-ASR.

Spin structure	M^{a}_{Mn} (μ_B)	M^{b}_{Mn} (μ_B)	M^{a}_{Rh} (μ_B)	M^{b}_{Rh} (μ_B)
$1Q$	2.57	2.54	0.04	−0.01
$2Q$	2.62	2.74	0.07	0.02
$3Q$	2.66	2.83	0.08	0.04

[a]TB-LMTO-CPA work by Sakuma *et al.*(Ref. 40).
[b]Present work.

using TB-LMTO-recursion.[34–36] In this communication we present a generalization of that technique for disordered alloys.

It appears that no detailed experimental investigation into noncollinear magnetism in either of the two disordered alloys has been carried out to confirm our predictions. We propose that such experiments be carried out so that we may confirm the theoretical predictions.

ACKNOWLEDGMENTS

We wish to thank Swedish Research Links program funded by VR/SIDA for supporting the project in which this work was carried out. O.E. and B.S. also acknowledge the Swedish Research Council (VR), ERC, and the Göran Gustafssons Foundation for financial support and the Swedish National Infrastructure for Computing (SNIC) for the allocation of supercomputing time.

[1] J. Kübler, K.-H. Höck, J. Sticht, and A. R. Williams, J. Phys. F: Metal Phys. **18**, 469 (1988).

[2] J. Sticht, K.-H. Höck, and J. Kübler, J. Phys. Condens. Matter **1**, 8155 (1989).

[3] M. Uhl, L. M. Sandratskii, and J. Kübler, Phys. Rev. B **50**, 291 (1994).

[4] R. Lorenz and J. Hafner, J. Magn. Magn. Matter. **139**, 139 (1995).

[5] Y. Kakehashi, S. Akbar, and N. Kimura, Phys. Rev. B **57**, 8354 (1998).

[6] T. C. Shulthess, W. H. Butler, G. M. Stocks, S. Maat, and G. J. Mankey, J. Appl. Phys. **15**, 4842 (1999).

[7] A. Sakuma, J. Phys. Soc. Jpn. **69**, 3072 (2000).

[8] A. Mookerjee, J. Phys. C: Solid State Phys. **6**, 1340 (1973).

[9] D. D. Koelling and B. N. Harmon, J. Phys. C: Solid State Phys. **10**, 3107 (1977).

[10] M. D. Stiles, S. V. Halilov, R. A. Hyman, and A. Zangwill, Phys. Rev. B **64**, 104430 (2001).

[11] G. Breit, Phys. Rev. **34**, 553 (1929); **36**, 383 (1930); **39**, 616 (1936).

[12] O. K. Andersen and O. Jepsen, Phys. Rev. L **53**, 2571 (1984).

[13] A. I. Lichtenstein, M. I. Katsnelson, V. P. Antropov, and V. A. Gubanov, J. Magn. Magn. Mater. **67**, 65 (1987).

[14] A. Mookerjee, in *Electronic Structure of Clusters, Surfaces and Disordered Materials*, edited by A. Mookerjee and D. D. Sarma (Taylor & Francis, London, 2003).

[15] A complex function $f(z)$ is called *Herglotz* if (a) its singularities lie on the real z axis, (b) $\mathrm{sgn}[\mathrm{Im}\, f(z)] = -\mathrm{sgn}(\mathrm{Im} z)$, and (c) $f(z) \sim 1/z$ as $z \to \pm\infty + i0$.

[16] A. Mookerjee and A. R. Bishop, J. Phys. C: Solid State Phys. **7**, 2165 (1974).

[17] S. S. A. Razee, A. Mookerjee, and R. Prasad, J. Phys. Condens. Matter **3**, 3301 (1991).

[18] V. Kumar, V. K. Srivastava, and A. Mookerjee, J. Phys. C: Solid State Phys. **15**, 1939 (1982).

[19] A. Mookerjee and R. Prasad, Phys. Rev. B **48**, 17724 (1993).

[20] T. Saha, I. Dasgupta, and A. Mookerjee, Phys. Rev. B **50**, 13267 (1994).

[21] A. Chakrabarti and A. Mookerjee, J. Phys. Condens. Matter **13**, 10149 (2001).

[22] T. Saha and A. Mookerjee, J. Phys. Condens. Matter **8**, 2915 (1996).

[23] R. Mills and P. Ratanavararaksa, Phys. Rev. B **18**, 5291 (1978).

[24] R. Mills, L. J. Gray, and T. Kaplan, Phys. Rev. B **27**, 3252 (1983).

[25] S. Ghosh, P. L. Leath, and M. H. Cohen, Phys. Rev. B **66**, 214206 (2002).

[26] A. Chakrabarti and A. Mookerjee, Europhys. J. B **44**, 21 (2005).

[27] R. Haydock, V. Heine, and M. J. Kelly, J. Phys. C: Solid State Phys. **5**, 2845 (1972).

[28] R. Haydock, in *Solid State Physics* (Academic Press, New York, 1980), Vol. 35.

[29] N. Beer and D. Pettifor, in *The Electronic Structure of Complex Systems* (Plenum Press, New York, 1984).

[30] A. Bergman, L. Nordström, A. B. Klautau, S. Frota-Pessoa, and O. Eriksson, Phys. Rev. B **73**, 174434 (2006).

[31] S. Frota-Pessôa, Phys. Rev. B **46**, 14570 (1992).

[32] C. M. M. Nex, Comp. Phys. Commun. **53**, 141 (1989).

[33] K. K. Saha and A. Mookerjee, J. Phys. Condens. Matter **17**, 287 (2005).

[34] A. Bergman, Ph.D. thesis, Uppsala University, Uppsala, Sweden.

[35] A. Bergman, L. Nordström, A. B. Klautau, S. Frota-Pessoa, and O. Eriksson, Surf. Sci. **600**, 4838 (2006).

[36] A. Bergman, L. Nordström, A. Burlamaqui Klautau, S. Frota-Pessoa, and O. Eriksson, Phys. Rev. B **75**, 224425 (2007).

[37] E. Kren, G. Kadar, L. Pal, J. Solyom, P. Szabo, and T. Tarnoczi, Phys. Rev. **171**, 574 (1968).

[38] A. V. Ruban and H. L. Skriver, Phys. Rev. B **66**, 024201 (2002).

[39] A. Sakuma, J. Magn. Magn. Mater. **187**, 105 (1998).

[40] A. Sakuma, R. Y. Umetsu, and K. Fukamichi, Phys. Rev. B **66**, 014432 (2002).

[41] E. F. Bertaut and D. Fruchart, Int. J. Magn. **2**, 259 (1972).

[42] S. Ghosh, N. Das, and A. Mookerjee, Int. J. Mod. Phys. B **21**, 723 (1999).